

# Electrochemistry of carbon dioxide corrosion mitigation using tall oil diethylenetriamine imidazoline as corrosion inhibitor for mild steel

I. Jevremović, M. Singer, S. Nešić and V. Mišković-Stanković\*

The inhibition effect of tall oil diethylenetriamine imidazoline (TOFA/DETA imidazoline) on corrosion of mild steel in CO<sub>2</sub>-saturated 3 wt% NaCl solution was investigated by electrochemical impedance spectroscopy (EIS), potentiodynamic sweep (PDS), cyclic voltammetry (CV), quartz crystal microbalance measurements (QCM), and scanning electron microscopy (SEM). TOFA/DETA imidazoline is a mixed-type corrosion inhibitor with the predominant anodic effect. The results of CV measurements indicate inhibited electrode processes in the presence of TOFA/DETA imidazoline and the absence of the rapid degradation of TOFA/DETA imidazoline in the range of mild steel corrosion potential. The corrosion rate of mild steel significantly decreased in the presence of TOFA/DETA imidazoline, while the inhibition efficiency increased up to 92%. It was found that the adsorption of studied imidazoline compound on steel surface followed both Langmuir and Temkin adsorption isotherms. The value of molecular interaction constant calculated from Temkin adsorption isotherm implied the existence of lateral repulsion between adsorbed inhibitor molecules.

## 1 Introduction

Carbon steel is the most commonly used material for construction of pipelines and associated production equipment. When dissolved in water, CO<sub>2</sub> is hydrated to form carbonic acid, the presence of which leads to a much higher corrosion rate of carbon steel than would be found in a solution of a strong acid at the same pH [1–6]. Carbonic acid enables hydrogen evolution at a much higher rate and serves as an additional source of hydronium ions. Another possible pathway, referred as “direct” reduction of carbonic acid, presumes carbonic acid adsorption at the steel surface followed by reduction of the hydronium ion [7–9]. Corrosion can be controlled to a great extent through design and selection of corrosion resistant materials, but capital costs can be significantly reduced with the use of lower alloyed steels in combination with an appropriate corrosion control practice [10]. The use of corrosion inhibitors is one of the most

practical and cost effective methods for combating CO<sub>2</sub> corrosion in oil and gas wells and flowlines [11]. A variety of organic compounds which generally contain nitrogen, oxygen, phosphorus, or sulfur heteroatoms act as corrosion inhibitors for steels. These compounds include amines, alkyl imidazoline salts, quaternary ammonium compounds, alkyl pyridinium salts, alkyl amides, triazoles, oxadiazoles, thiourea derivatives, thiosemicarbazide, thiocyanates, and the combinations thereof [12–17].

Imidazoline-based corrosion inhibitors are cationic surface active compounds widely used for protecting pipelines from CO<sub>2</sub> corrosion in the oil and gas industry [18–21]. The surfactants have an affinity to accumulate at the interface of immiscible fluids resulting in a corresponding lowering of the interfacial tension. Due to their surfactant nature, corrosion inhibitors adsorb at the interface between two phases such as air and water, oil and water, or solution and metal electrode and form a protective barrier against corrosive agents at the metal surface. The surface-active properties of corrosion inhibitors originate from their amphiphilic molecular structure comprised of a polar head group and a non-polar hydrophobic tail [22,23]. The polar head group possesses a high affinity for a mild steel substrate through either non-specific (physisorption) or specific (chemisorption) processes. It was reported that adsorption of corrosion inhibitors could also occur through hydrogen bonding [24]. Due to its hydrophobic character, the hydrocarbon chain effectively disperses water and aqueous species from the steel surface.

I. Jevremović, V. Mišković-Stanković

Faculty of Technology and Metallurgy, University of Belgrade, Karnegijeva 4, 11000 Belgrade (Serbia)  
E-mail: vesna@tmf.bg.ac.rs

M. Singer, S. Nešić

Institute for Corrosion and Multiphase Technology, Ohio University, 342 West State St. Athens, OH 45701 (USA)

Ultimately, the effectiveness of organic inhibitors is related to the extent to which they adsorb and cover the metal surface. Adsorption depends on the chemical structure of the inhibitor, on the nature and surface charge of the metal surface, and on the type of corrosive environment [25]. It is reported that the peak inhibition of corrosion with organic corrosion inhibitors is attained at the critical micelle concentration (CMC) of a particular compound, where aggregation of monomers into micelles occurs. The CMC is a property of a surfactant nature, concentration, temperature, pH, pressure, and ionic strength of the solution [26,27].

The aim of the present study was to investigate adsorption and corrosion inhibition mechanism of TOFA/DETA imidazoline on mild steel in CO<sub>2</sub>-saturated 3 wt% NaCl solution as well as the stability and surface morphology of inhibitor film. In this work, the inhibition and adsorption behavior of TOFA/DETA imidazoline in CO<sub>2</sub>-saturated 3 wt% NaCl solution was investigated using potentiodynamic sweep (PDS), cyclic voltammetry (CV), and electrochemical impedance spectroscopy (EIS) technique, while the surface morphology of mild steel in the presence and absence of TOFA/DETA imidazoline was studied by scanning electron microscopy (SEM). To further confirm these findings in the present study, inhibition effect of TOFA/DETA imidazoline was also investigated using quartz crystal microbalance (QCM) measurements. Impedance data was used to define the adsorption isotherm and to calculate the thermodynamic parameters.

Molecular structure of TOFA/DETA imidazoline is depicted in Fig. 1, where it can be seen that the inhibitor molecule consists of three different substructures: a nitrogen-containing five member ring, a pendant side chain with a hydrophilic active functional group (ethylamino pendent group) attached to N1 and a long C-17 hydrophobic chain attached to the C2 atom. The term TOFA is intended to define tall oil fatty acids with oleic acid as a major component.

## 2 Experimental

### 2.1 Materials

X65 carbon steel was used for the corrosion measurements. Its composition (mass% balance is Fe) is 0.13C, 0.26Si, 1.15Mn, 0.32Al, 0.16Mo, 0.36Ni, 0.131Cu, <0.009S, <0.009P. Tall oil diethylenetriamine imidazoline (TOFA/DETA imidazoline),

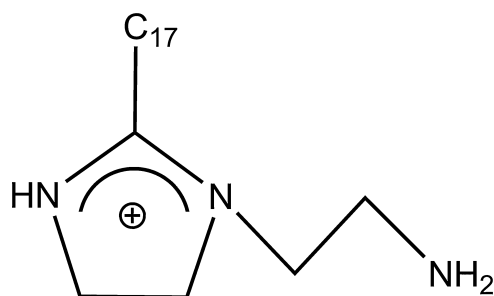


Figure 1. Molecular structure of TOFA/DETA imidazoline

tested in the present study, was prepared by reacting tall oil fatty acid (TOFA), a mixture of oleic and linoleic acids with an equimolar amount of diethylene triamine (DETA). TOFA/DETA imidazoline is a water dispersible corrosion inhibitor with molecular weight of 359 g/mol, while its density and viscosity measured at 25 °C are 980 kg/m and 200 mPa/s, respectively.

### 2.2 Electrochemical measurements

Experiments were conducted using a conventional three-electrode cell assembly. The rotating cylinder test specimens (5.4 cm<sup>2</sup> exposed area), machined from X65 pipeline steel, were used as the working electrode. A platinum mesh was used as the counter electrode and a saturated silver/silver chloride (Ag/AgCl) reference electrode was connected externally via a Luggin capillary tube. The test specimens were grinded sequentially using 240, 320, 400, and 600 grit silicon carbide paper, degreased with isopropanol in an ultrasonic water bath and dried with hot air. Experiments were conducted under stagnant conditions at atmospheric pressure, at different temperatures in the range from 20 to 50 °C. Test solution was 3 wt% NaCl. The solutions were deoxygenated by purging CO<sub>2</sub> gas for 1 h before the start of the experiment. A positive pressure of CO<sub>2</sub> was maintained in the cell during the experiments, minimizing the possibility of air ingress. TOFA/DETA imidazoline was introduced into the solution in the concentration range from 50 to 90 ppm<sub>v</sub> after the bare steel corrosion tests had been conducted. All the electrochemical measurements were carried out using a reference 600 TM Potentiostat/Galvanostat/ZRA (Gamry Instruments, Inc. Warminster, PA, USA), while the impedance spectra were analyzed using the Gamry Instruments Echem Analyst fitting procedure. EIS and PDS measurements were carried out subsequently after 30 min of open-circuit potential, *E*<sub>ocp</sub>, measurements.

#### 2.2.1 PDS measurements

The PDS measurements were carried out from a cathodic potential of -0.25 V to an anodic potential of 0.25 V with respect to the corrosion potential, at a scan rate of 1 mV/s.

#### 2.2.2 CV measurements

The stability of the inhibitor film, formed on the metal surface, was also examined by CV measurements. In order to investigate TOFA/DETA imidazoline oxidation resistance and its influence on the cathodic process, the CV tests were performed first on a platinum working electrode, then on mild steel electrode, considering that the platinum electrode allows the recording of cyclic voltammograms in the wider potential range especially in the anodic domain. In order to study corrosion inhibitor adsorption, two platinum electrodes (9 × 10 mm<sup>2</sup>) were used as working and counter electrodes, and Ag/AgCl as a reference electrode. Subsequently, carbon steel coupons (exposed area of 5.4 cm<sup>2</sup>) were employed as working electrodes in order to evaluate the corrosion inhibitor adsorption on a corroding metal surface. The cyclic voltammograms on platinum were first obtained in 1 M H<sub>2</sub>SO<sub>4</sub> solution deaerated by means of nitrogen without and with 90 ppm<sub>v</sub> of TOFA/DETA imidazoline and then in CO<sub>2</sub>-saturated 3 wt% NaCl test solution without and with

90 ppm<sub>v</sub> of TOFA/DETA imidazoline. All the experiments were performed at 20 °C. The procedure of CV tests on platinum electrode was as follows: specimen conditioning at 0.2 V *versus* Ag/AgCl for 60 s in order to clean the surface, followed by 10 consecutive voltammetry cycles from -0.2 V to +1.05 V *versus* Ag/AgCl at 100 mV/s scan rate. Cyclic voltammograms of carbon steel electrodes with and without corrosion inhibitor were recorded in the potential region between -1.0 V and -0.6 V *versus* Ag/AgCl at a scan rate of 20 mV/s, starting from the open circuit potential,  $E_{ocp}$ . In each experiment, cycling was continued until stabilized voltammograms were obtained (typically 4 cycles).

### 2.2.3 EIS measurements

The EIS measurements were carried out over a frequency range from 10 kHz to 10 mHz using a 10 mV amplitude of sinusoidal variation around the  $E_{ocp}$ . The data obtained from the EIS measurements were also used to discuss the inhibitor adsorption and inhibition mechanism.

### 2.3 QCM measurements

Further adsorption measurements were carried out using a quartz crystal microbalance controller, QCM200, coupled with a QCM25 crystal oscillator (Stanford Research Systems, USA) loaded with Au/Fe sensor quartz crystals (2.54 cm diameter, AT-

cut, Stanford Research Systems). The fundamental oscillation frequency of the used crystals was 5 MHz. The solutions were deaerated by purging CO<sub>2</sub> gas during the whole test in order to maintain positive CO<sub>2</sub> partial pressure and the pH of the test solution was adjusted to 5. Experiments were performed at 20 °C. Once the desired conditions were achieved, the QCM crystal was immersed in the solution and the change of the oscillation frequency,  $\Delta f$ , was recorded for 1 h.

### 2.4 Surface morphology

A scanning electron microscope (JEOL JSM-6390) was used to analyze the morphology of mild steel surface. Images of the specimens were recorded after 24 h exposure time in 3 wt% NaCl purged with CO<sub>2</sub> gas at 20 °C, and at 70 °C without and with 90 ppm<sub>v</sub> of TOFA/DETA imidazoline.

## 3 Results and discussion

### 3.1 PDS measurements

Potentiodynamic polarization curves recorded for mild steel in CO<sub>2</sub>-saturated 3 wt% NaCl solution without and with varying concentrations of TOFA/DETA imidazoline at different temperatures in the range from 20 to 50 °C are shown in Fig. 2.

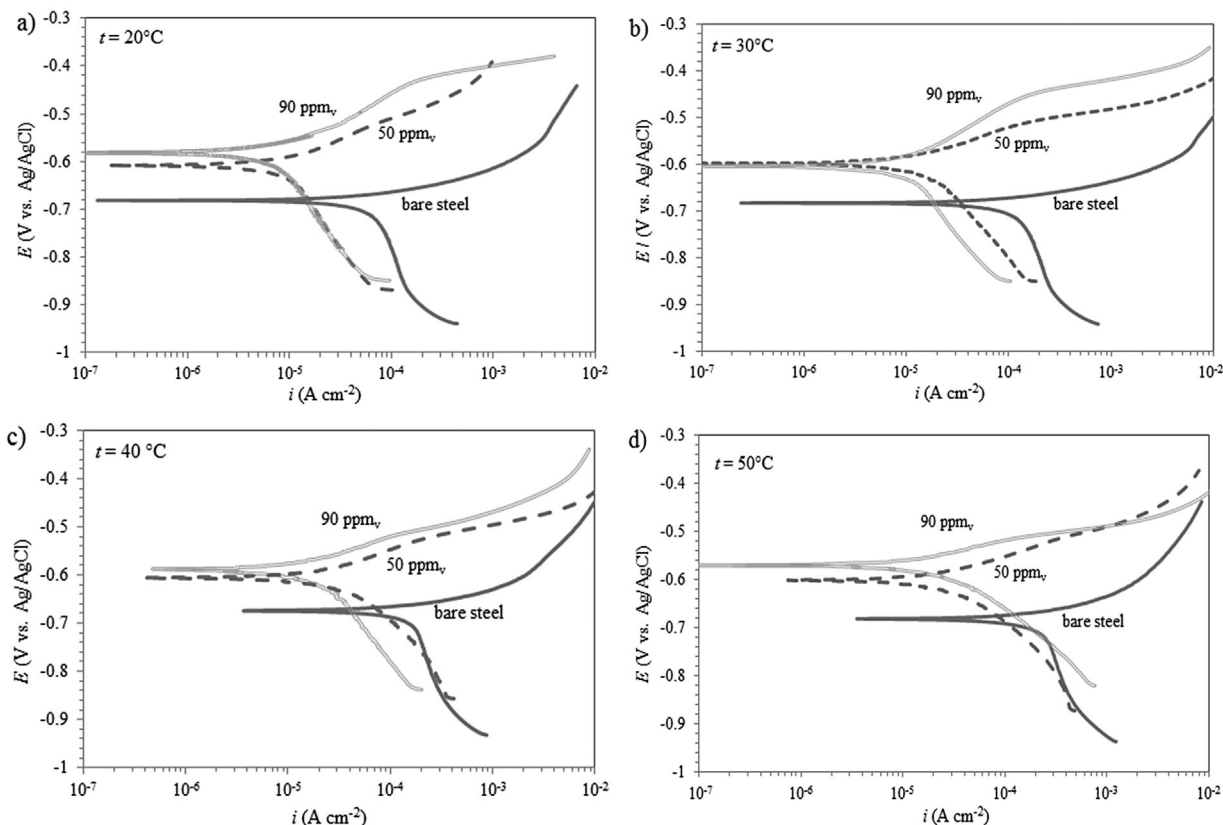


**Figure 2.** Polarization curves of mild steel in 3 wt% NaCl solution with varying concentrations of TOFA/DETA imidazoline at: a) 20 °C, b) 30 °C, c) 40 °C, and d) 50 °C

As can be seen in Fig. 2, the corrosion rate of bare steel in 3 wt% NaCl saturated with CO<sub>2</sub> is governed by the cathodic reaction mechanism. It is widely accepted that the mechanism of mild steel corrosion in CO<sub>2</sub>-saturated brine is under both mass transfer and activation control [28]. The cathodic limiting current is commonly attributed to the superposition of the diffusion limited reduction of H<sup>+</sup> and H<sub>2</sub>CO<sub>3</sub>. It was reported that at pH 5, the dominant cathodic reaction is H<sub>2</sub>CO<sub>3</sub> reduction while the contribution of H<sup>+</sup> was much smaller than at lower pH. The slow replenishment of the H<sub>2</sub>CO<sub>3</sub> and consequently the limiting current for this reaction is controlled by the slow hydration of dissolved CO<sub>2</sub> [7]. The change of slope of the cathodic curve at high overpotentials corresponds to direct H<sub>2</sub>O reduction. It is reported that the anodic dissolution of iron is affected by the presence of CO<sub>2</sub>, where carbonic species in solution are acting as chemical ligands and catalyzing the dissolution of iron [29]. The addition of TOFA/DETA imidazoline shifts the corrosion potential to more positive values and decreases the corrosion current density of mild steel while the shifts are dependent on the inhibitor concentration. It can be also noticed that the current density increased with increasing temperature in the presence and absence of corrosion inhibitor due to the acceleration of all the processes involved in corrosion. According to Fig. 2, the presence of TOFA/DETA imidazoline affects both anodic and cathodic partial reaction with a more noticeable anodic effect. Consequently, TOFA/DETA imidazoline can be considered a mixed-type inhibitor, with the predominant influence on the anode process due to the adsorption of the inhibitor molecules on the corresponding active sites. At potentials higher than -0.4 V versus Ag/AgCl, the change of slope of the anodic curve and the increase of anodic current density are observed. This behavior was already reported for iron and can be explained by desorption of adsorbed inhibitor molecules and the decrease of the degree of coverage of the electrode surface with increasing anodic potential [30–33]. Desorption from the metal surface upon anode polarization is typical for many organic compounds, including imidazolines [13]. It was also reported that the second anodic slope, observed at higher overpotentials, is related to desorption of the strongly adsorbed halide ions, while the surface of the metal is dominated by adsorbed FeOH [34]. The corrosion

current density was determined graphically by the intersection of the extrapolated Tafel region of the anodic and the cathodic polarization curves. Values of kinetic parameters extracted from the polarization curves including anodic and cathodic Tafel constants,  $b_a$  and  $b_c$ , corrosion potential,  $E_{\text{corr}}$ , corrosion current density,  $i_{\text{corr}}$ , corrosion rate,  $v_{\text{corr}}$ , and inhibition efficiency,  $\eta$  (%) are listed in Table 1. Corrosion rate,  $v_{\text{corr}}$  and inhibition efficiency,  $\eta$  (%) were calculated using the following equations, respectively:

$$v_{\text{corr}} = \frac{M}{nF\rho} i_{\text{corr}} \quad (1)$$

$$\eta (\%) = \frac{i_{\text{corr}}^0 - i_{\text{corr}}}{i_{\text{corr}}^0} \times 100 \quad (2)$$

where  $M$  is molar mass of Fe (55.845 g/mol),  $\rho$  is the density (7.874 g/cm<sup>3</sup>),  $n$  is the charge number which indicates the number of electrons exchanged in the dissolution reaction,  $F$  is the Faraday constant, (96 485 C/mol),  $i_{\text{corr}}^0$  and  $i_{\text{corr}}$  are corrosion current densities of mild steel in 3 wt% NaCl solution without and with TOFA/DETA imidazoline, respectively, determined by extrapolation of Tafel lines to the corrosion potential.

By assessing Table 1 data, a significant decrease in  $i_{\text{corr}}$  and consequently  $v_{\text{corr}}$  with the increasing concentrations of TOFA/DETA imidazoline is apparent, leading to the increase of inhibition efficiency,  $\eta$  (%) up to 92%. The shift of  $E_{\text{corr}}$  value to more noble values indicates that the inhibitor can effectively inhibit the anodic dissolution of mild steel in CO<sub>2</sub>-saturated chloride solution. However,  $i_{\text{corr}}$  increased with increasing temperature due to corrosion process acceleration with increasing temperature, while the temperature had no significant effect on the inhibitor efficiency. In CO<sub>2</sub> corrosion, the determination of Tafel slopes is not straightforward due to the complexity of the polarization curves. As can be seen in Table 1, almost infinite value of  $b_c$  and the value of  $b_a$  close to 40 mV/dec were observed for bare steel in 3 wt% NaCl saturated with CO<sub>2</sub>, at all given temperatures. This is consistent with  $b_a$  values (40–60 mV/dec) typically reported for iron dissolution controlled by charge

**Table 1.** Electrochemical data obtained from the potentiodynamic curves at different temperatures carried out on carbon steel in 3 wt% NaCl solution saturated with CO<sub>2</sub> with varying concentrations of TOFA/DETA imidazoline

$t$ (°C)	$c$ (ppm <sub>v</sub> )	$b_a$ (mV/dec)	$-b_c$ (mV/dec)	$i_{\text{corr}}$ (10 <sup>4</sup> A/cm <sup>2</sup> )	$E_{\text{corr}}$ (mV vs. Ag/AgCl)	$\theta$	$\eta$ (%)
20	–	39	590	0.64	–679	–	–
	50	80	306	0.084	–608	0.87	87
	90	110	280	0.066	–582	0.90	90
30	–	40	443	1.10	–683	–	–
	50	70	250	0.146	–603	0.87	87
	90	114	278	0.087	–602	0.92	92
40	–	40	454	1.47	–674	–	–
	50	68	190	0.250	–606	0.83	83
	90	64	273	0.140	–587	0.90	90
50	–	39	490	2.10	–681	–	–
	50	60	174	0.245	–601	0.89	89
	90	47	165	0.175	–570	0.92	92

transfer [35]. It can be observed that both cathodic and anodic Tafel constants increased with TOFA/DETA imidazoline concentration.

The influence of temperature on the rate of corrosion reaction can be further discussed using the Arrhenius equation, which defines the corrosion current density,  $i_{\text{corr}}$ , as a function of the activation energy,  $E_a$  [36–38].

$$i_{\text{corr}} = A \exp\left(-\frac{E_a}{RT}\right) \quad (3)$$

where  $T$  is the temperature,  $A$  is the pre-exponential factor, and  $R$  is the gas constant. The activation energy is the excess energy that must be acquired to transform metal atoms at the metal surface into solvated metal ions. Figure 3 represents plot of  $\log i_{\text{corr}}$  versus  $1/T$  for mild steel in  $\text{CO}_2$  saturated 3 wt% NaCl solution in the absence and presence of different TOFA/DETA imidazoline concentrations.

Values of the apparent activation energy of corrosion for mild steel were determined from the slope of  $\log i_{\text{corr}}$  versus  $1/T$  plots. The calculated activation energy values in the absence and presence of 50 and 90 ppm<sub>v</sub> of TOFA/DETA imidazoline are 30.4, 29.8, and 26.7 kJ/mol, respectively. The obtained  $E_a$  value in the absence of corrosion inhibitor in  $\text{CO}_2$ -saturated chloride solution is close to the previously reported values [39]. In the presence of TOFA/DETA imidazoline,  $\eta$  (%) slightly increases with temperature, leading to small decrease in  $E_a$ . The decrease in  $E_a$  in the presence of inhibitor can indicate a partial chemical adsorption of TOFA/DETA imidazoline on the mild steel surface [40–42]. According to some authors, the increase in  $\eta$  (%) with increasing temperature can be explained by specific interactions established between the metal surface and the corrosion inhibitor. Lower activation energy in the inhibited solution can be the result of the inhibitor adsorption on the sites of higher activation energy, while the surface sites with lower activation energy stay unoccupied. This way adsorbed inhibitor molecules shield the active sites on the metal surface therefore lowering the  $E_a$  of the corrosion process [43].

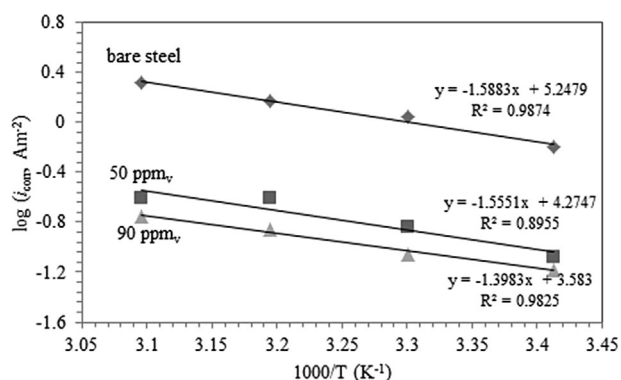


**Figure 3.** Arrhenius plots of  $\log i_{\text{corr}}$  versus  $1/T$  for carbon steel in  $\text{CO}_2$ -saturated 3 wt% NaCl solution without and with different concentrations of TOFA/DETA imidazoline

### 3.2 CV measurements

The stability of TOFA/DETA imidazoline and its electrochemical behavior was further investigated by CV measurements. The voltammetry tests were performed first on a platinum working electrode in order to extend the potential domain. The CV analysis was performed for platinum electrode in 1 M  $\text{H}_2\text{SO}_4$  solution, in order to obtain the typical hydrogen adsorption/desorption profile of platinum, and then in  $\text{CO}_2$ -saturated 3 wt% NaCl aqueous solution, in order to get better insight into the corrosion inhibitor adsorption process. Figure 4 shows the cyclic voltammograms of platinum electrode in 1 M  $\text{H}_2\text{SO}_4$  solution in the presence and absence of 90 ppm<sub>v</sub> of TOFA/DETA imidazoline. The measurements were carried out with a scan rate of 100 mV/s.

The electrode was first subjected to potential cycles until all unstable atoms or clusters were removed and a reproducible hydrogen adsorption/desorption peak was obtained, as depicted in Fig. 4. The base curve obtained in the absence of the inhibitor presents the typical cyclic voltammogram at a large polycrystalline platinum electrode in acidic media [44,45]. A broad current increase in the potential range from 0.60 to 1.15 V versus Ag/AgCl (B) can be assigned to oxygen release and to platinum oxide growth, while a broad cathodic peak at about 0.55 V (C), originates from platinum oxide reduction formed during the anodic sweep. Cathodic peak (D) and its anodic counterpart (E) in the potential region from -0.20 to 0.10 V versus Ag/AgCl correspond to hydrogen adsorption/desorption on the platinum electrode surface [46]. Addition of TOFA/DETA imidazoline in a test solution leads to a less visible hydrogen adsorption and desorption peaks as well as to the decrease of oxygen release peak. As can be seen in Fig. 4, in the presence of TOFA/DETA imidazoline all the reactions are inhibited, due to the adsorption of inhibitor molecules on platinum electrode active sites.

Subsequently, the cyclic voltammograms of platinum electrode in  $\text{CO}_2$ -saturated 3 wt% NaCl solution devoid of and containing 90 ppm<sub>v</sub> of TOFA/DETA imidazoline were recorded (Fig. 5).

As depicted in Fig. 5, the cyclic voltammetric response on a bare platinum electrode in 3 wt% NaCl solution saturated with

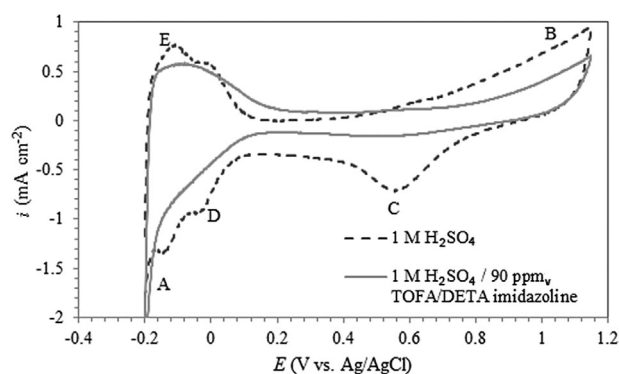


**Figure 4.** Cyclic voltammograms obtained in 1 M  $\text{H}_2\text{SO}_4$  at platinum electrode with and without 90 ppm<sub>v</sub> of TOFA/DETA imidazoline, 20 °C, scan rate 100 mV/s

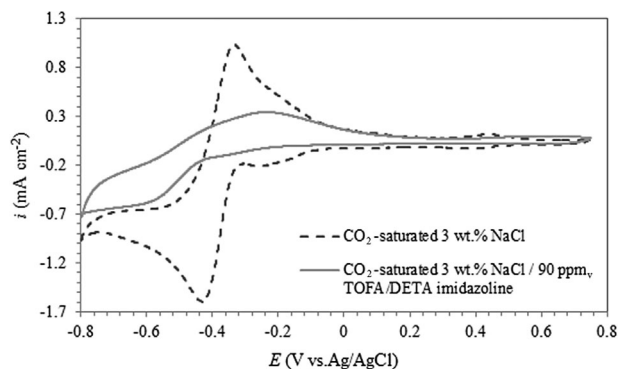


**Figure 5.** Cyclic voltammograms obtained in  $\text{CO}_2$ -saturated 3 wt% NaCl solution at platinum electrode with and without 90 ppm<sub>v</sub> of TOFA/DETA imidazoline, 20 °C, scan rate 100 mV/s

$\text{CO}_2$  and the one obtained after the addition of TOFA/DETA imidazoline are visibly different. Cyclic voltammogram recorded in the presence of TOFA/DETA imidazoline exhibited peaks with significantly lower current intensity, confirming the inhibitor surface film formation. Electroreduction of  $\text{CO}_2$  on polycrystalline platinum is an irreversible interaction of  $\text{CO}_2$  molecules activated as a result of weak adsorption on the metal surface with chemisorbed hydrogen. The exact nature of chemisorbed particles formed during  $\text{CO}_2$  electroreduction is still debatable and several studies [47,48] focused on the identification of the  $\text{CO}_2$  reduction products. A discussion of these is beyond the scope of the present research.

The cyclic voltammograms of carbon steel in 3 wt% NaCl solution devoid of and containing 90 ppm<sub>v</sub> of TOFA/DETA imidazoline were recorded and are represented in Fig. 6.

As can be seen in Fig. 6, in the case of bare mild steel in 3 wt% NaCl solution an anodic potential shoulder (B) starting at about  $-0.65$  V versus Ag/AgCl corresponds to oxidation of steel [49]. Further on, the anodic current increased continuously with increasing potential (C) indicating active dissolution of steel. Also a cathodic current peak (A) detected at about  $-0.94$  V versus Ag/AgCl was attributed to the reduction of iron oxide product present on the steel surface, which was formed during

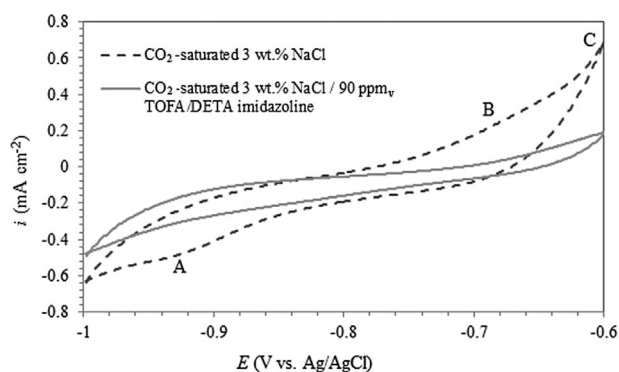


**Figure 6.** Cyclic voltammograms obtained in  $\text{CO}_2$ -saturated 3 wt% NaCl solution at mild steel electrode with and without 90 ppm<sub>v</sub> of TOFA/DETA imidazoline, 20 °C, scan rate 20 mV/s

the positive potential scanning [50]. The presence of inhibitor in the test solution significantly reduces cathodic and anodic current density. It can be observed that upon the addition of TOFA/DETA imidazoline, there is no additional reaction identified in the cyclic voltammogram. Thereby, it can be concluded that the electrode processes are inhibited due to the physical adsorption of the corrosion inhibitor on the mild steel surface. Formed inhibitor film creates a barrier for charge and mass transfer. As depicted in Fig. 6, TOFA/DETA imidazoline does not undergo major changes, indicating that the rapid degradation of TOFA/DETA imidazoline does not occur in the range of mild steel corrosion potential.

### 3.3 EIS measurements

The Nyquist plots and the corresponding Bode plots of mild steel in  $\text{CO}_2$ -saturated 3 wt% NaCl solution with and without TOFA/DETA imidazoline in the concentration range from 50 to 90 ppm<sub>v</sub> at different temperatures (20–50 °C) are shown in Figs. 7 and 8, respectively.

A comparison of Nyquist plots reveals that the impedance significantly increases with addition of TOFA/DETA imidazoline and is dependent on the concentration of the TOFA/DETA imidazoline indicating the inhibition of the corrosion process. The presence of single peaks in the phase-angle plots (Fig. 8) indicates a single time constant while the continuous increase in the phase angle shift and the peak width with the increase in TOFA/DETA imidazoline concentration indicate a more capacitive response of the interface due to the adsorption of inhibitor molecules. In the presence of different concentrations of TOFA/DETA imidazoline, the single phase is broadening and shifting to lower frequencies while the phase angle slightly increases at higher concentrations of TOFA/DETA imidazoline due to the formation of protective barrier against aggressive ions from the bulk solution at the mild steel surface. The values of phase angles lower than  $90^\circ$  may indicate that the corrosion process is under mixed control (diffusion and charge transfer).

The EIS data were analyzed using a simple electrical equivalent circuit as shown in Fig. 9, where  $R_\Omega$  is the solution resistance,  $R_{ct}$  represents the charge-transfer resistance, and CPE is the constant phase element, which represents all the frequency-dependent electrochemical phenomena, namely double-layer capacitance,  $C_{dl}$ , and diffusion processes [51]. The CPE quantifies different physical phenomena like surface roughness, inhibitor adsorption, and porous layer formation. It can be also considered that the inhibitor layer resistance is much smaller than the charge-transfer resistance, therefore EIS data in the complex plain could not be analyzed by fitting to an equivalent electrical circuit model representing two time constants. Two time constants are not distinguished in Nyquist diagram due to the overlapping of inhibitor layer and charge-transfer loop, although at higher inhibitor concentrations the Bode plots (Fig. 8a–d) show slight deviation at 10 000 Hz, which undoubtedly indicates the existence of TOFA/DETA imidazoline layer on the electrode. One possible explanation could be the formation of TOFA/DETA imidazoline monolayer on the mild steel surface [52].

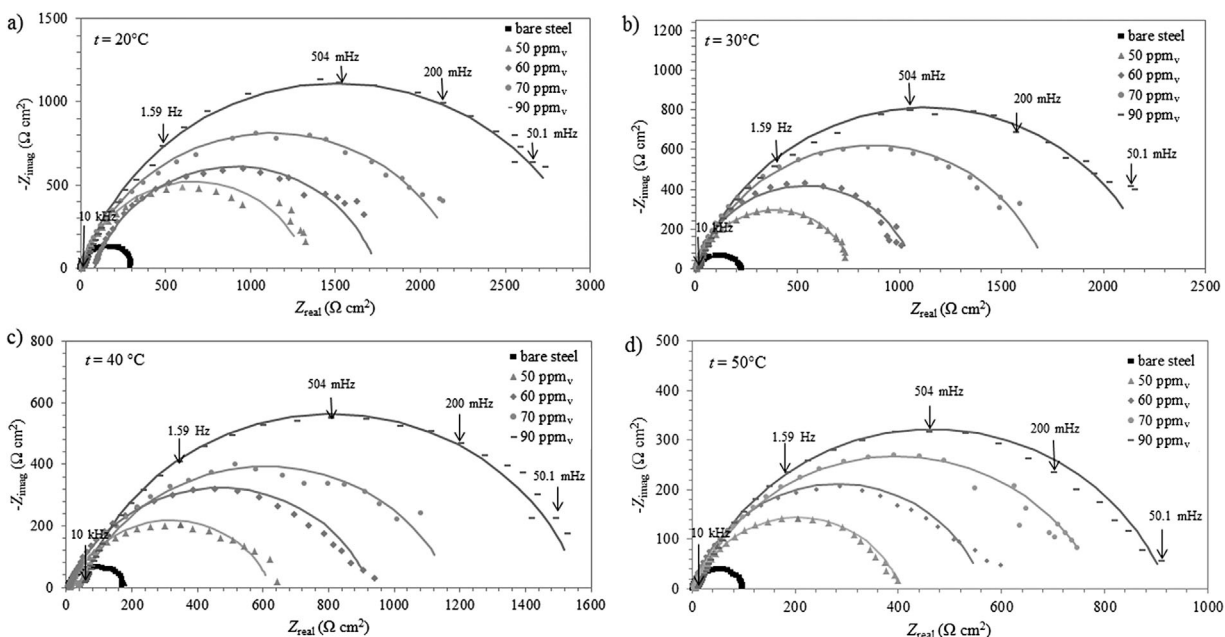


**Figure 7.** Nyquist plots (experimental) and the fitting curves (solid lines) for mild steel in  $\text{CO}_2$ -saturated 3 wt% NaCl solution with and without different concentrations of TOFA/DETA imidazoline at: a) 20 °C, b) 30 °C, c) 40 °C, and d) 50 °C

CPE is used in this model to compensate non-homogeneity in the system and is defined by two parameters,  $Y_0$  and  $n$ . The impedance of CPE is defined using the following equation:

$$Z_{\text{CPE}} = Y_0^{-1} (j\omega)^{-n} \quad (4)$$

where  $Y_0$  and  $n$  are the CPE constant and exponent, respectively,  $\omega$  is the angular frequency in  $\text{rad s}^{-1}$  ( $\omega = 2\pi f$ ) and  $j^2 = -1$  is an imaginary number. If  $n$  values range from 0.8 to 1, the impedance of CPE can be considered to be the one of the pure capacitor [53–55]:

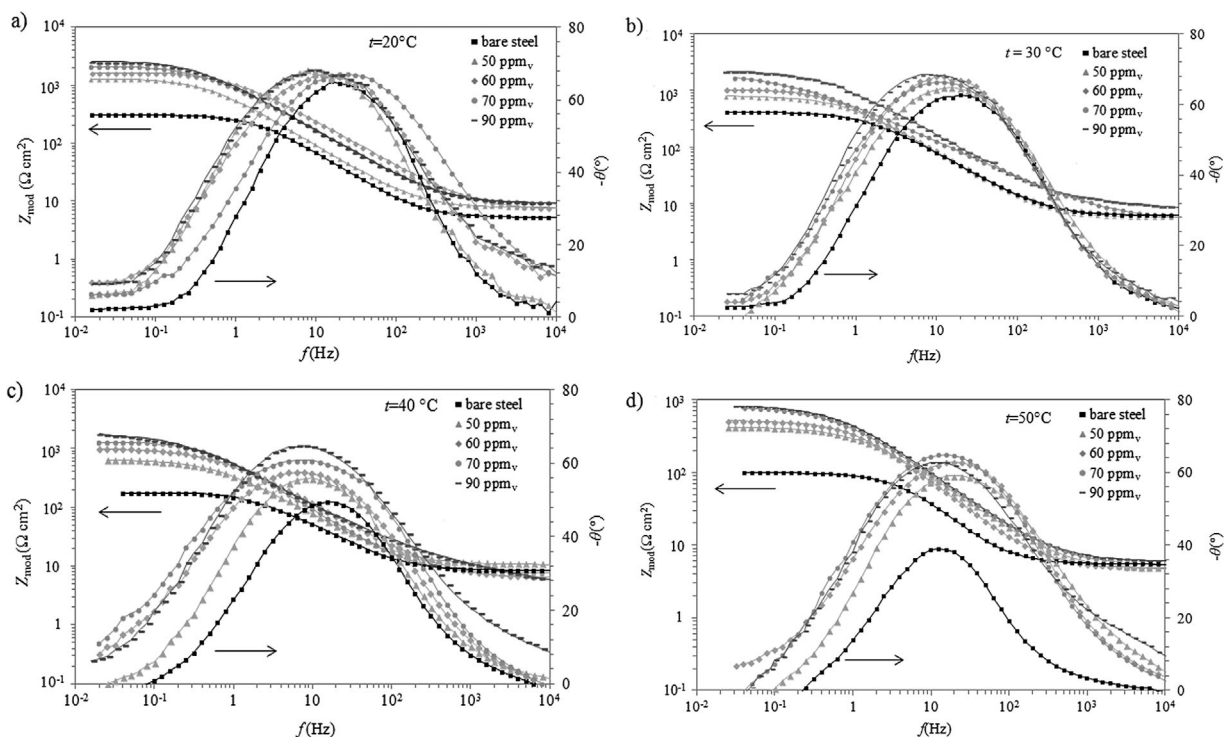


**Figure 8.** Bode plots for mild steel in  $\text{CO}_2$ -saturated 3 wt% NaCl solution with and without different concentrations of TOFA/DETA imidazoline at: a) 20 °C, b) 30 °C, c) 40 °C, and d) 50 °C

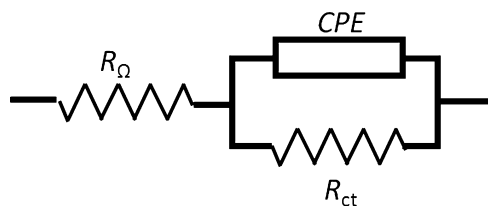


Figure 9. Electrical equivalent circuit

$$Z_{CPE} = (j\omega C)^{-n} \quad (5)$$

and in this case  $Y_0$  gives a pure capacitance ( $C$ ).

The impedance data in the complex plane were well fitted by the proposed EEC and we used three basic criteria to evaluate the general accuracy of the fit: visual fit to Bode and Nyquist plots, low goodness of fit, and low relative standard errors for every circuit element [56]. We obtained suitably low goodness of fit ( $<10^{-4}$ ) and the error associated with each element lower than 5%. Therefore, it can be concluded that the chosen fit describes investigated systems accurately.

The surface coverage,  $\theta$ , and the inhibition efficiency,  $\eta$  (%), were then calculated from the following equations, respectively:

$$\theta = \frac{R_{ct} - R_{ct}^0}{R_{ct}} \quad (6)$$

$$\eta (\%) = \frac{R_{ct} - R_{ct}^0}{R_{ct}} \times 100 \quad (7)$$

where  $R_{ct}^0$  and  $R_{ct}$  are the charge-transfer resistance values without and with inhibitor, respectively. The values of

charge-transfer resistance,  $R_{ct}$ , obtained from the fitting procedure, constant phase element parameter,  $n$ , double-layer capacitance,  $C_{dl}$ , surface coverage,  $\theta$ , and inhibition efficiency,  $\eta$  (%) are listed in Table 2. Given that all the values of parameter  $n$  shown in this table are greater than 0.8, the values of  $C_{dl}$  have been calculated instead of CPE.

As can be seen in Table 2, the values of charge-transfer resistance increase and the values of double-layer capacitance decrease with increasing inhibitor concentration due to the gradual replacement of water molecules by inhibitor molecules at the metal surface. The inhibition efficiency  $\eta$  (%) of TOFA/DETA imidazoline increases with increasing its concentration from 20 to 90 ppm<sub>v</sub> up to 90% change much with its concentration. The decrease in double-layer capacitance with increase in TOFA/DETA imidazoline comes from a decrease in a local dielectric constant due to the formation of a protective inhibitor layer on mild steel surface. The thickness of this protective layer increases with increase in inhibitor concentration resulting in a decrease in double layer-capacitance. On the other hand, increase in temperature decreases the values of charge-transfer resistance and increases the values of double-layer capacitance due to the increased corrosion rate at higher temperatures. The inhibition efficiency values obtained from the EIS measurements (Table 2) are in accordance with those obtained from the PDS measurements (Table 1).

### 3.3.1 Thermodynamic parameters

Values of the degree of surface coverage,  $\theta$ , obtained from EIS measurements were used to determine the adsorption isotherm. The experimental results have been fitted to a series of adsorption isotherms and it was found that the adsorption of studied imidazoline compound on steel surface obeys Langmuir adsorption isotherm:

Table 2. The values of charge-transfer resistance, double-layer capacitance, surface coverage, and inhibition efficiency obtained from EIS measurements for mild steel in 3 wt% NaCl without and with inhibitor at different temperatures

$t$ (°C)	$c_{inh}$ (ppm <sub>v</sub> )	$R_{ct}$ ( $\Omega$ cm <sup>2</sup> )	$\theta$	$\eta$ (%)	$C_{dl}$ ( $\mu$ F/cm <sup>2</sup> )	$n$
20	Bare steel	307	–	–	374	0.877
	50	1326	0.769	76.9	355	0.847
	60	1659	0.815	81.5	328	0.809
	70	2239	0.863	86.3	219	0.799
	90	3005	0.897	89.7	203	0.811
30	Bare steel	219	–	–	724	0.837
	50	761	0.712	71.2	449	0.838
	60	1059	0.794	79.4	355	0.850
	70	1752	0.875	87.5	326	0.764
	90	2215	0.901	90.1	218	0.810
40	Bare steel	177	–	–	715	0.792
	50	624	0.717	71.7	522	0.794
	60	935	0.811	81.1	354	0.799
	70	1122	0.843	84.3	332	0.784
	90	1521	0.883	88.3	317	0.813
50	Bare steel	98	–	–	716	0.842
	50	399	0.752	75.2	596	0.795
	60	566	0.825	82.5	531	0.816
	70	785	0.874	87.4	452	0.763
	90	916	0.891	89.1	340	0.880

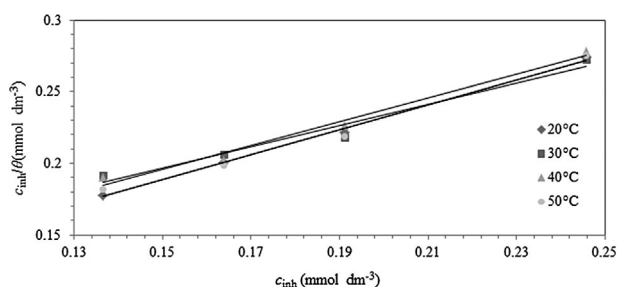


**Figure 10.** Langmuir adsorption isotherm for mild steel in CO<sub>2</sub>-saturated 3 wt% NaCl solution in the presence of TOFA/DETA imidazoline at different temperatures

$$\frac{c_{\text{inh}}}{\theta} = \frac{1}{K_{\text{eq}}} + c_{\text{inh}} \quad (8)$$

where  $c_{\text{inh}}$  is the concentration of inhibitor,  $K_{\text{eq}}$  the adsorption equilibrium constant, and  $\theta$  is the surface coverage. Figure 10 depicts the straight lines of  $c_{\text{inh}}/\theta$  versus  $c_{\text{inh}}$  with good linear relationship.

The slight deviation of the slopes from unity indicates the existence of interactions between adsorbed and adsorbing molecules. The size of the hydrophobic chain in TOFA/DETA imidazoline molecule could result in significant steric hindrance for adsorbing molecules. In order to further examine the detected interactions between the adsorbed inhibitor molecules, Temkin adsorption isotherm was also tested. Temkin adsorption isotherm is given by the following equation [57]:

$$\theta = \frac{1}{f} \ln K_{\text{eq}} + \frac{1}{f} \ln c_{\text{inh}} \quad (9)$$

where  $f$  is the Temkin heterogeneity factor. Frumkin interaction parameter  $a$  is related to the Temkin heterogeneity factor by the following relation [58]:

$$f = -2a \quad (10)$$

Frumkin interaction parameter  $a$  ( $a=0$ , no interaction;  $a > 0$ , attraction;  $a < 0$ , repulsion) is dependent on the hydrophilic head group charge, hydrophobic chain length, flexibility, or

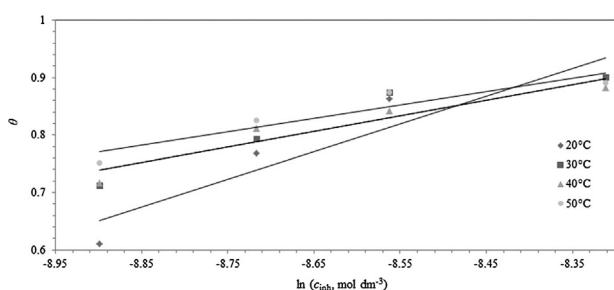


**Figure 11.** Temkin adsorption isotherm for mild steel in CO<sub>2</sub>-saturated 3 wt% NaCl solution in the presence of TOFA/DETA imidazoline at different temperatures

**Table 3.** The values of  $K_{\text{eq}}$  and  $\Delta G_{\text{ads}}^{\circ}$  determined from Langmuir adsorption isotherm as a function of temperature

$t$ (°C)	$T$ (K)	Linear correlation coefficient ( $r$ )	$K_{\text{eq}}$ ( $10^3 \text{ M}^{-1}$ )	$\Delta G^{\circ}$ (kJ/mol)
20	293.15	0.99	17.79	-23.85
30	303.15	0.96	11.76	-23.62
40	313.15	0.98	13.99	-24.85
50	323.15	0.98	17.33	-26.22

branching [57,59]. Figure 11 depicts the straight lines of  $\theta$  versus  $\ln c_{\text{inh}}$  with good linear relationship.

Standard Gibbs free energy of adsorption,  $\Delta G_{\text{ads}}^{\circ}$  was determined from the following equation:

$$\Delta G_{\text{ads}}^{\circ} = -RT \ln K_{\text{eq}} \quad (11)$$

where  $R$  is the gas constant and  $T$  is the absolute temperature. Calculated values of  $K_{\text{eq}}$  and  $\Delta G_{\text{ads}}^{\circ}$  determined from Langmuir and Temkin adsorption isotherm are summarized in Tables 3 and 4, respectively.

The mild steel surface is negatively charged in the chloride solution and therefore adsorption of positively charged (cationic) corrosion inhibitor is facilitated. Although it is difficult to differentiate chemisorption and physisorption processes only based on the values of  $\Delta G_{\text{ads}}^{\circ}$ , according to the literature [60–62] the calculated values of  $\Delta G_{\text{ads}}^{\circ}$  may indicate that the adsorption of TOFA/DETA imidazoline is governed by physisorption mechanism. In order to determine standard entropy of adsorption,  $\Delta S_{\text{ads}}^{\circ}$ , at any given temperature, the change in standard Gibbs free energy of adsorption,  $\Delta G_{\text{ads}}^{\circ}$ , may be written from the definition of the Gibbs free energy as [63]:

$$\Delta G_{\text{ads}}^{\circ} = \Delta H_{\text{ads}}^{\circ} - T \Delta S_{\text{ads}}^{\circ} \quad (12)$$

where  $\Delta H_{\text{ads}}^{\circ}$  standard enthalpy of adsorption. The temperature dependences of  $\Delta G_{\text{ads}}^{\circ}$  for adsorption of TOFA/DETA imidazoline in the temperature range from 293 to 323 K for both Langmuir and Temkin adsorption isotherms are shown in Fig. 12.

From Langmuir adsorption isotherm, the value of  $\Delta S_{\text{ads}}^{\circ}$  was calculated to be 83.4 J/mol/K, while  $\Delta H_{\text{ads}}^{\circ}$  was 1.07 kJ/mol. From Temkin adsorption isotherm,  $\Delta S_{\text{ads}}^{\circ}$  was calculated to be

**Table 4.** The values of  $K_{\text{eq}}$ ,  $\Delta G_{\text{ads}}^{\circ}$ , and  $f$  determined from Temkin adsorption isotherm as a function of temperature

$t$ (°C)	$T$ (K)	Linear correlation coefficient ( $r$ )	$K_{\text{eq}}$ ( $10^4 \text{ M}^{-1}$ )	$\Delta G^{\circ}$ (kJ/mol)	$f$	$a$
20	293.15	0.87	2.84	-24.99	2.08	-1.04
30	303.15	0.91	6.82	-28.05	3.06	-1.53
40	313.15	0.91	11.21	-30.27	3.70	-1.85
50	323.15	0.88	19.43	-32.72	4.26	-2.13

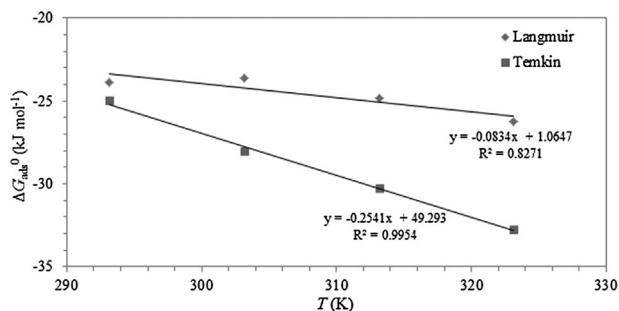


**Figure 12.** Temperature dependences of  $\Delta G_{\text{ads}}^{\circ}$  for adsorption of TOFA/DETA imidazoline on mild steel surface in the temperature range from 293 to 325 K for Langmuir and Temkin adsorption isotherms

254.1 J/mol/K, whereas  $\Delta H_{\text{ads}}^{\circ}$  was 49.3 kJ/mol. The obtained positive values of  $\Delta H_{\text{ads}}^{\circ}$  and  $\Delta S_{\text{ads}}^{\circ}$  indicate that the adsorption process of TOFA/DETA imidazoline on mild steel surface is endothermic and driven by entropy gain associated with the exchange of water molecules with inhibitor molecules on the metal surface [64]. The adsorption of an organic inhibitor on the metal/electrolyte interface is followed by the gradual replacement of water, molecules initially adsorbed on the metal surface, by the organic molecules in the aqueous solution. In the case of adsorption from solution, inhibitor molecule upon adsorption loses  $3^{\circ}$  of translational freedom that it had in the solution, while the desorbed water gains  $3^{\circ}$  of translational freedom. Consequently, the exchange of  $n$  water molecules from the metal surface due to the adsorption of an organic molecule leads to  $3n-3$ , the difference in number of translational degrees of freedom. Dehydration processes of strongly structured interfacial water and adsorption of larger inhibitor molecules at the surface will cause  $\Delta S_{\text{ads}}^{\circ}$  in the system to increase, compensating the increase in enthalpy.

Frumkin interaction parameter  $a$  is an average of the total attraction and repulsion forces among the adsorbed molecules [39]. The negative sign of this constant, calculated from Temkin adsorption isotherm (Table 4), implies the existence of lateral repulsion between adsorbed species. According to the obtained results of the electrochemical measurements, a

discussion of the most likely adsorption mechanism of TOFA/DETA imidazoline inhibitor film on mild steel surface from  $\text{CO}_2$ -saturated 3 wt% NaCl solution can be presumed. TOFA/DETA imidazoline molecules can be adsorbed on the mild steel surface by electrostatic interaction between the negative charge on the metal surface in chloride medium and the positive charge on the imidazoline ring. Physically adsorbed TOFA/DETA imidazoline compound is shielding the part of the negative charge on the metal surface, consequently shifting the corrosion potential toward more positive values. In addition to the physical adsorption, a donor–acceptor surface complex can be also established by interaction of the p-system of aromatic ring in TOFA/DETA imidazoline and a vacant d-orbital of metal. The inhibitor molecules can also adsorb on the steel surface by formation of Fe–N co-ordination bond. Therefore, it can be assumed that the imidazoline ring and nitrogen heteroatom are the active sites of TOFA/DETA imidazoline corrosion inhibitor while the hydrocarbon chain can form hydrophobic film and protect the metal surface from corrosive species. Based on these results, TOFA/DETA imidazoline was judged to display good inhibiting properties against  $\text{CO}_2$  corrosion.

### 3.4 QCM measurements

Inhibitor adsorption and formation of a protective layer on the metal surface was further observed on an iron-coated quartz crystal. QCM measures the mass difference due to the metallic corrosion and replacement of water by inhibitor molecules [65]. QCM frequency change recorded with time was converted to mass change using Sauerbrey's equation. The linear correlation between mass and frequency is described by the Sauerbrey equation, as shown below:

$$\Delta f = -\frac{2f_0^2}{\sqrt{\mu_q \rho_q}} \Delta m \quad (13)$$

where  $\Delta f$  is the resonant frequency shift,  $\Delta m$  is the change in mass per unit area,  $f_0$  is the fundamental frequency of the resonator,  $\rho_q$ , the density of the quartz crystal, and  $\mu$  is the shear modulus of the quartz crystal [66].

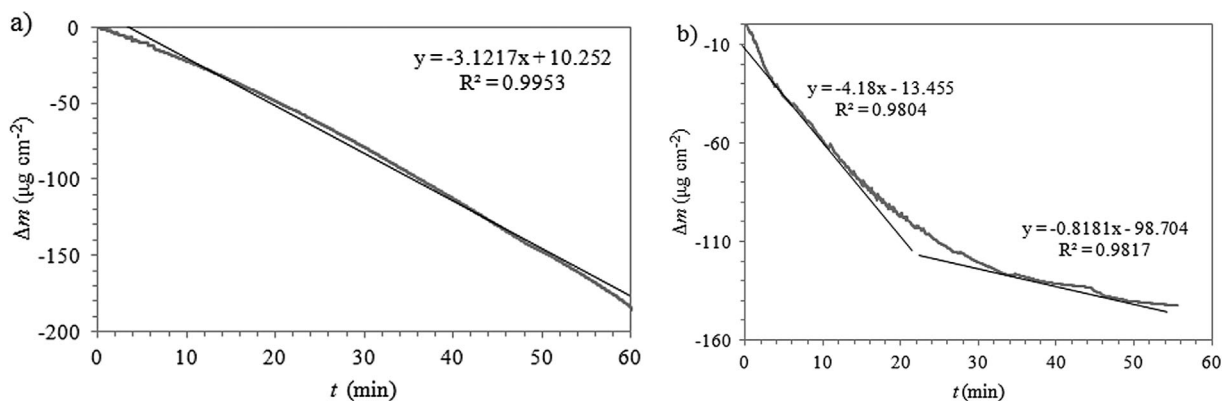


**Figure 13.** The mass versus time curve for iron-coated quartz crystal in  $\text{CO}_2$ -saturated 3 wt% NaCl solution: a) without and b) with 90 ppm, of TOFA/DETA imidazoline, pH = 5, 20 °C

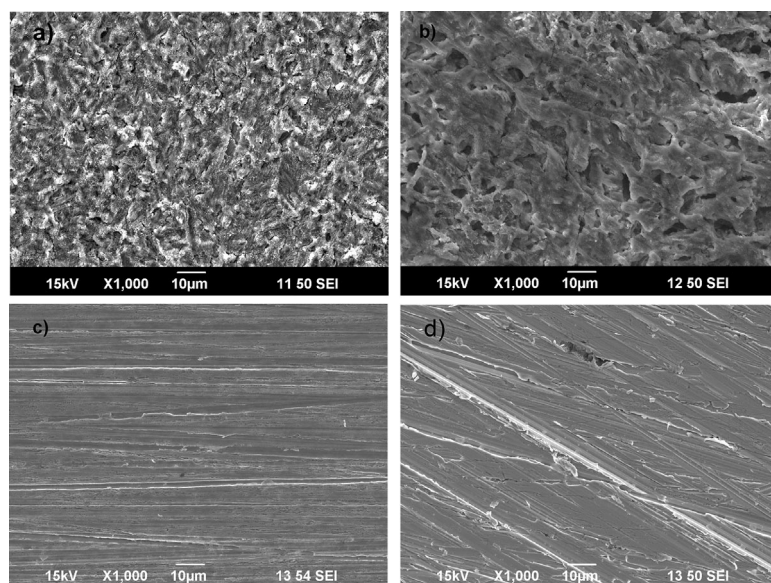


**Figure 14.** SEM images of the mild steel surface exposed to 3 wt% NaCl solution saturated with CO<sub>2</sub> without: a) at 20 °C, b) at 70 °C and with 90 ppm<sub>v</sub> of TOFA/DETA imidazoline: c) at 20 °C, d) at 70 °C

Figure 13 shows the change in the mass of iron-coated quartz crystal immersed in 3 wt% NaCl solution saturated with CO<sub>2</sub>, pH = 5 at 20 °C without and with 90 ppm<sub>v</sub> of TOFA/DETA imidazoline for 1 h.

The exposure of an iron-coated quartz crystal to CO<sub>2</sub>-saturated 3 wt% NaCl solution without TOFA/DETA imidazoline for 1 h led to a mass decrease of 180 µg/cm<sup>2</sup>, due to iron dissolution. The linear regression was used to fit metal thickness loss data to a linear relationship and to determine the value of corrosion rate. The obtained mass decrease with time is almost linear with a slope of  $-3.12 \mu\text{g}/\text{cm}^2/\text{min}$  (Fig. 13a). The acquired value corresponds to corrosion rate of 2.1 mm/y. As can be seen in Fig. 13b, the sharp decrease in mass that occurs in the first 20 min of the electrode exposure to chloride solution containing TOFA/DETA imidazoline corresponds to corrosion rate of 2.8 mm/y. The decrease in mass stops after approximately 20 min and the corrosion rate decreases to 0.54 mm/y probably due to the growth of corrosion inhibitor film on iron-coated crystal involving replacement of water from the crystal surface. Initial mass loss can be attributed to the replacement reaction between inhibitor and water molecules at the quartz crystal–solution interface [67].

### 3.5 Surface morphology

Surface examination of mild steel exposed to the test solutions and further investigation of the corrosion protection of TOFA/DETA imidazoline was carried out by means of scanning electron microscopy (SEM). Microphotographs of mild steel surface after 24 h of exposure to 3 wt% NaCl solutions without and with TOFA/DETA imidazoline at 20 °C and at 70 °C are shown in Fig. 14.

In the absence of inhibitor (Fig. 14a and b), the mild steel surface was strongly damaged due to metal dissolution in the

corrosive solution. A large number of pits and cracks distributed over the surface appeared. Nevertheless, the appearance of steel surface was significantly improved after the introduction of TOFA/DETA imidazoline to the corrosive solution. It is clearly evident that the surface is more uniform and less damaged than the surface in the absence of the inhibitor. Figure 14c and d clearly shows that the corrosion rate of mild steel decreased and very flat surface appeared, suggesting that TOFA/DETA imidazoline forms an inhibitive film on the mild steel surface which is very stable and protective even at elevated temperatures after 24 h exposure to the aggressive solution. These results support the results of the electrochemical measurements which are discussed above.

## 4 Conclusions

The investigated organic compound TOFA/DETA imidazoline exhibited high inhibition efficiency against mild steel corrosion in 3 wt% NaCl solution saturated with CO<sub>2</sub>. It was assumed that the imidazoline ring and nitrogen heteroatom are the active sites of TOFA/DETA imidazoline corrosion inhibitor while the hydrocarbon chain forms hydrophobic film and protect the metal surface from corrosive species. The protection efficiency increased with increasing inhibitor concentration from 50 to 90 ppm<sub>v</sub>, up to 94% efficiency. PDS measurements show that TOFA/DETA imidazoline can be considered a mixed-type corrosion inhibitor with the predominant anodic effect. The addition of TOFA/DETA imidazoline decreased the corrosion current density for more than one order of magnitude. The results of CV measurements indicate inhibited electrode processes in the presence of TOFA/DETA imidazoline due to the adsorption of inhibitor molecules on mild steel electrode active sites. EIS measurements revealed that the thickness of

TOFA/DETA imidazoline protective layer increases with increase in inhibitor concentration resulting in a decrease in double layer-capacitance. The calculated values of standard Gibbs free energy, standard entropy, and standard enthalpy of adsorption indicated that the adsorption of studied imidazoline compound on steel surface is governed by physisorption mechanism and follows both Langmuir and Temkin adsorption isotherm at all studied temperatures. The data fitted to the Temkin adsorption isotherm provided additional information, compared to the Langmuir adsorption isotherm, in the form of a molecular interaction constant, which implied the existence of lateral repulsion between adsorbed inhibitor molecules. QCM measurements proved that corrosion rate of iron-coated quartz crystal decreased to 0.54 mm/y in the presence of inhibitor compared to corrosion rate of 2.1 mm/y without inhibitor. These results show the efficiency of the TOFA/DETA imidazoline in the CO<sub>2</sub>-saturated 3 wt% NaCl solution as a result of the interaction that takes place between the inhibitor and the metal surface.

**Acknowledgments:** The authors would like to express their gratitude to ConocoPhillips, USA, and the Ministry of Education, Science, and Technological Development, Republic of Serbia (grant no. III 45019) for the financial support.

## 5 References

- [1] Q. Y. Liu, L. J. Mao, S. W. Zhou, *Corros. Sci.* **2014**, *56*, 165.
- [2] C. De Waard, D. E. Milliams, *Corrosion*, **1975**, *31*, 177.
- [3] G. I. Ogundele, W. E. White, *Corrosion*, **1986**, *42*, 71.
- [4] P. C. Okafor, S. Nešić, *Chem. Eng. Comm.* **2007**, *194*, 141.
- [5] F. Vitse, S. Nešić, Y. Gunaltun, D. L. de Torreben, P. Duchet-Suchaux, *Corrosion* **2003**, *59*, 1075.
- [6] Z. Zhang, D. Hinkson, M. Singer, H. Wang, S. Nešić, *Corrosion* **2007**, *63*, 1051.
- [7] S. Nešić, J. Postlethwaite, S. Olsen, *Corrosion* **1996**, *52*, 280.
- [8] S. Nešić, L. Lunde, *Corrosion* **1994**, *50*, 717.
- [9] M. Nordsveen, S. Nešić, R. Nyborg, A. Stangeland, *Corrosion* **2003**, *59*, 443.
- [10] D. M. Ortega-Toledo, J. G. Gonzalez-Rodriguez, M. Casales, L. Martinez, A. Martinez-Villafañe, *Corros. Sci.* **2011**, *53*, 3780.
- [11] S. H. Yoo, Y. W. Kim, K. Chung, S. Y. Baik, J. S. Kim, *Corros. Sci.* **2012**, *54*, 42.
- [12] G. Žerjav, I. Milošev, *Mater. Corros.* **2016**, *67*, 92.
- [13] V. S. Reznik, V. D. Akamsin, Y. P. Khodyrev, R. M. Galiakberov, Y. Y. Efremov, L. Tiwari, *Corros. Sci.* **2008**, *50*, 392.
- [14] M. Finšgar, I. Milošev, *Corros. Sci.* **2010**, *52*, 2737.
- [15] M. Finšgar, J. Kovač, I. Milošev, *J. Electrochem. Soc.* **2010**, *157*, C52.
- [16] M. Finšgar, J. Jackson, *Corros. Sci.* **2014**, *86*, 17.
- [17] I. Jevremović, A. Debeljković, M. Singer, M. Achour, S. Nesic, V. Mišković-Stanković, *J. Serbian Chem. Soc.* **2012**, *77*, 1047.
- [18] I. Jevremović, M. Singer, M. Achour, D. Blumer, T. Baugh, V. Mišković-Stanković, S. Nešić, *Corrosion*, **2013**, *69*, 186.
- [19] I. Jevremović, M. Singer, S. Nešić, V. Mišković-Stanković, *Corros. Sci.* **2013**, *77*, 265.
- [20] G. Zhang, C. Chen, M. Lu, C. Chai, Y. Wu, *Mater. Chem. Phys.* **2007**, *105*, 331.
- [21] J. Cruz, R. Martínez, J. Genesca, E. García-Ochoa, *J. Electroanal. Chem.* **2004**, *566*, 111.
- [22] S. Ramachandran, V. Jovancevic, *Corrosion* **1999**, *55*, 259.
- [23] X. Zhang, F. Wang, Y. He, Y. Du, *Corros. Sci.* **2001**, *43*, 1417.
- [24] F. Branzoi, V. Branzoi, C. Licu, *Mater. Corros.* **2014**, *65*, 637.
- [25] M. Dūdūkcū, *Mater. Corros.* **2011**, *62*, 264.
- [26] F. Schreiber, *Prog. Surf. Sci.* **2000**, *65*, 151.
- [27] V. Jovancevic, S. Ramachandran, P. Prince, *Corrosion* **1999**, *55*, 449.
- [28] S. Nešić, B. F. M. Pots, J. Postlethwaite, N. Thevenot, *J. Corr. Sci. Eng.* **1995**, *1*, 1.
- [29] S. Nešić, *Corros. Sci.* **2007**, *49*, 4308.
- [30] F. Y. Cui, L. Guo, S. T. Zhang, *Mater. Corros.* **2014**, *65*, 1194.
- [31] A. A. Aksüt, W. J. Lorenz, F. Mansfeld, *Corros. Sci.* **1982**, *22*, 611.
- [32] R. Yıldız, A. Döner, T. Doğan, İ. Dehri, *Corros. Sci.* **2014**, *82*, 125.
- [33] A. Zarrouk, B. Hammouti, T. Lakhli, M. Traisnel, H. Vezin, F. Bentiss, *Corros. Sci.* **2015**, *90*, 572.
- [34] P. C. Okafor, Y. Zheng, *Corros. Sci.* **2009**, *51*, 850.
- [35] M. Knag, K. Bilkova, E. Gulbrandsen, P. Carlsen, J. Sjöblom, *Corros. Sci.* **2006**, *48*, 2592.
- [36] L. Wang, S. W. Zhang, Q. Guo, H. Zheng, D. M. Lu, L. Peng, *Mater. Corros.* **2015**, *66*, 594.
- [37] D. E. J. Talbot, J. D. R. Talbot, *Corrosion Science and Technology*, CRC Press, London **1997**.
- [38] H. Kaesche, *Corrosion of Metals: Physicochemical Principles and Current Problems*, Springer, Berlin, Heidelberg **2003**.
- [39] M. P. Desimone, G. Gordillo, S. N. Simison, *Corros. Sci.* **2011**, *53*, 4033.
- [40] M. A. Amin, M. A. Ahmed, H. A. Arida, T. Arslan, M. Saracoglu, F. Kandemirli, *Corros. Sci.* **2011**, *53*, 540.
- [41] S. Deng, X. Li, X. Xie, *Corros. Sci.* **2014**, *80*, 276.
- [42] F. Bentiss, M. Traisnel, N. Chaibi, B. Mernari, H. Vezin, M. Lagrenée, *Corros. Sci.* **2002**, *44*, 2271.
- [43] A. Popova, E. Sokolova, S. Raicheva, M. Christov, *Corros. Sci.* **2003**, *45*, 33.
- [44] D. Zhan, J. Velmurugan, M. V. Mirkin, *J. Am. Chem. Soc.* **2009**, *131*, 14756.
- [45] G. S. Attard, P. N. Bartlett, N. R. B. Coleman, J. M. Elliott, J. R. Owen, J. H. Wang, *Science* **1997**, *278*, 838.
- [46] M. W. Breiter, *J. Phys. Chem.* **1964**, *68*, 2249.
- [47] Y. B. Vassiliev, V. S. Bagotzky, N. V. Osetrova, A. A. Mikhailova, *J. Electroanal. Chem. Interfacial Electrochem.* **1985**, *189*, 311.
- [48] T. Smolinka, M. Heinen, Y. X. Chen, Z. Jusys, W. Lehnert, R. J. Behm, *Electrochim. Acta.* **2005**, *50*, 5189.
- [49] L. Niu, Y. F. Cheng, *Appl. Surf. Sci.* **2007**, *253*, 8626.
- [50] Y. Cheng, *Int. J. Hydrogen Energy.* **2007**, *32*, 1269.
- [51] K. Bílková, E. Gulbrandsen, *Electrochim. Acta.* **2008**, *53*, 5423.
- [52] M. Heydari, M. Javidi, *Corros. Sci.* **2012**, *61*, 148.
- [53] M. Sluyters-Rehbach, *Pure Appl. Chem.* **1994**, *66*, 1831.
- [54] V. D. Jović, B. M. Jović, *J. Electroanal. Chem.* **2003**, *541*, 1.
- [55] M. M. Popović, B. N. Grgur, V. B. Mišković-Stanković, *Prog. Org. Coatings* **2005**, *52*, 359.
- [56] M. E. Orazem, B. Tribollet, *Electrochemical Impedance Spectroscopy*, John Wiley & Sons, New York **2011**.

- [57] W. Durnie, *J. Electrochem. Soc.* **1999**, *146*, 1751.
- [58] D. M. M. Dražić, L. Vračar, V. J. J. Dražić, *Electrochim. Acta.* **1994**, *39*, 1165.
- [59] A. Popova, M. Christov, A. Vasilev, A. Zwetanova, *Corros. Sci.* **2011**, *53*, 679.
- [60] F. Zhang, Y. Tang, Z. Cao, W. Jing, Z. Wu, Y. Chen, *Corros. Sci.* **2012**, *61*, 1.
- [61] J. Aljourani, K. Raeissi, M. A. Golozar, *Corros. Sci.* **2009**, *51*, 1836.
- [62] E. S. Meresht, T. S. Farahani, J. Neshati, *Corros. Sci.* **2012**, *54*, 36.
- [63] B. G. Ateya, B. E. El-Anadouli, F. M. El-Nizamy, *Corros. Sci.* **1984**, *24*, 509.
- [64] J. Zhang, X. L. Gong, H. H. Yu, M. Du, *Corros. Sci.* **2011**, *53*, 3324.
- [65] A. Yurt, Ö. Aykın, *Corros. Sci.* **2011**, *53*, 3725.
- [66] B. Binks, D. Furlong, *Modern Characterization Methods of Surfactant Systems (Surfactant Science)*, CRC Press, Boca Raton **1999**.
- [67] P. Kern, D. Landolt, *Corros. Sci.* **2002**, *44*, 1809.

(Received: August 29, 2015)

W8629

(Accepted: October 5, 2015)